Welding in the World (2022) 66:1665–1673
https://doi.org/10.1007/s40194-022-01313-5

RESEARCH PAPER

Microstructure and mechanical properties of Al–Mg-Sc-Zr welded joint

S. H. Wen[1,2] · H. J. Jiao[1] · L. G. Zhou[1] · Q. S. Zhang[1] · S. J. Wu[2]

Received: 9 October 2021 / Accepted: 3 May 2022 / Published online: 1 June 2022

Abstract
The Al–Mg-Sc-Zr alloy was welded using three kinds of weld filler wires containing different additions of zirconium, scandium, titanium, and boron. With a uniform Al_3(Sc,Zr) and TiB_2 dispersed on the α-Al matrix in the fusion zone, the Al–Mg-Sc-Zr-TiB_2 weld displayed the best tensile property, its yield strength and tensile strength of welded joint with reinforcement reached 232.2 MPa and 386.3 MPa, and the yield strength and tensile strength of weld without reinforcement was about 208.0 MPa and 358.4 MPa, respectively. The fractions of the Al_3(Sc,Zr) phase in the fusion zone was relative to the Sc and Zr content. A remarkable grain refining effect was observed for addition of Zr, Sc, and TiB_2, because the formation of Al_3(Sc,Zr) and TiB_2 can act as nucleant particles during solidification. With the increase of Sc/Zr and TiB_2 addition in the melting fusion, the tensile strength, yield strength, and corresponding elongation of the 2195 Al-Li alloy increase, while the impact toughness slightly decreases.

Highlights

- **The Al–Mg-Sc-Zr welded joint manly consists of the α-Al matrix, TiB_2 particles, and Al_3(Sc, Zr) precipitates.**
- **The finer Al_3(Sc, Zr) particles dispersed on the α-Al matrix in the heat-affected zone.**
- **The Al_3(Sc, Zr) and TiB_2 particles have the main effects of refining the grain size in the fusion zone.**
- **The tensile strength and yield strength of the Al–Mg-Sc-Zr welded joint increase with the increase of grain refiner content in the fusion.**

Keywords Al–Mg-Sc alloy · Welding · Microstructure · Mechanical properties · Grain refinement

1 Introduction

1.1 Background

Non-heat-treatable Al–Mg alloys (5xxx serious) are widely used in the field of chemical industries because of their attractive properties such as high ductility and good corrosion resistance [1–5]. The main strengthening mechanism in Al–Mg alloys is cold work in addition to a small amount of solid solution strengthening. The disadvantage of the Al–Mg alloys is their relatively low strength compared to the precipitation-hardened aluminum alloys such as Al-Cu alloys (2xxx serious). An effective approach to enhance the strength of Al alloys is the addition of alloying elements. Aluminum alloys are usually grain refined by Al-Ti, Al-Ti-B, Al-Zr, and Al-Sc alloys, which provide heterogeneous nucleation sites such as $TiAl_3$, TiB_2, Al_3Zr, and Al_3Sc particles. Schempp and Cross [6–15] have proved that the grain refinement is an effective approach to improve the mechanical properties of fusion welds and the weldability of the Al alloy. Al–Mg-Sc alloys are based on Al–Mg alloys with the addition of scandium [16–19]. Scandium can be combined with aluminum to form a stable Al_3Sc precipitate with the Ll_2 structure. These uniform Al_3Sc particles dispersed on the aluminum matrix reduce the grain size [20, 21]. In addition, the nanoscaled coherent Al_3Sc has the same crystal structure

Recommended for publication by Commission XI—Pressure Vessels, Boilers, and Pipelines.

✉ S. J. Wu
wusj@buaa.edu.cn

[1] Aerospace Research Institute of Materials & Processing Technology, Beijing 100076, China

[2] School of Materials Science and Engineering, Beihang University, Xueyuan Road No. 37, Beijing 100191, China

and similar lattice parameters as the α-Al matrix, resulting in a coherent strengthening effect. Therefore, Al–Mg-Sc alloy has a higher ultimate strength and excellence weldability with low hot crack susceptibility [22–26].

1.2 Literature review

Previous studies indicated that the yield strength and welding coefficient (the ratio of tensile strength of welded joint to tensile strength of the base metal) of the Al–Mg-Sc weldments were still low. For example, the Al–Mg-Sc-Zr plates with 6-mm thickness in H32 were welded by variable polarity plasma arc welding (VPPAW) using a Sc- and Zr-containing filler wire [23]. The yield strength, tensile strength, and elongation of the welded joint with reinforcement were 188 MPa, 330 MPa, and 9.5%, respectively. The welding coefficient was only 74% in this test. The microstructure and mechanical properties of the arc welded joints of the Al–Mg-Sc plate were studied by Fu [26]. The rolled plates of Al-6 Mg-0.25Sc-0.4Mn-0.12Zr (wt.%) alloy with 2-mm thickness was fusion welded using the gas tungsten arc weld technique. The results showed that the yield strength and ultimate tensile strength were 238 MPa and 338 MPa, respectively. The decrease in the tensile strength between TIG joint and the base material was almost 30%.

Adjusting the constituent of weld filler wires is the most effective approach to improve the mechanical properties of the Al–Mg-Sc alloys. The microstructure and mechanical properties of the Al–Mg-Sc welded joint with 2-mm thickness prepared by the metal inert gas (MIG) welding method using an A1-6.5 Mg-0.4(Sc,Zr) weld filler wire as fusion materials were investigated [27]. The fine equal-axed grains in the fusion zone improved the strength of the welded joint, while the coefficients of weld strength with reinforcement were greater than 0.90. The tensile strength of Al–Mg-(Sc,Zr) alloy plates was about 380 MPa, and the elongation was higher than 7%. However, the dependence of mechanical properties of the welded joint without reinforcement on the element content in weld filler wires has not been systematically investigated.

In this work, Al–Mg-Sc-Zr alloy was welded by tungsten inert gas arc welding using three types of weld filler wires. These filler metals containing different additions of Sc, Zr, and TiB_2 were developed to improve the mechanical properties of the welded joint. With a determination of the dilution ratio and base material, the compositions of the welded joint could be quantitatively controlled by adjusting the original compositions of the weld filler wires. After welding, the microstructure and mechanical properties of the welded joint were investigated. The effect of Sc, Zr, and TiB_2 on the microstructure and mechanical performance of Al–Mg-Sc-Zr weldment with reinforcement and without reinforcement was discussed.

2 Material and experimental procedures

2.1 Materials

The 6-mm-thick cold-rolled Al–Mg-Sc alloy plate with the nominal chemical compositions (wt. %) of 6.2 Mg, 0.3 Sc, 0.1 Zr, and balance Al was used as base material. The cold work deformation of the plate is 8%. Three types of weld filler wires were developed in order to enhance the mechanical properties of the Al–Mg-Sc-Zr welded joint. In this work, the button ingots Al–Mg-Sc-Zr-(Ti-B) alloy were prepared using a tungsten arc–melting furnace. Pure Al, Mg, Al-2Sc, Al-5Zr, KBF_4, and K_2TiF_6 were placed into the furnace, and the in situ TiB_2 particles were formed during the melting process. Then, the button ingots were extruded to the weld filler wires. These weld filler wires with 3.0-mm diameter were Al-based alloy containing different alloying elements such as Zr, Sc, Ti, and B, identifying as S5000, S5001, and S5002. The nominal chemical compositions (wt. %) of the weld filler wires are listed in Table 1.

2.2 Welding procedure

The welding specimens were machined to the dimension of 300 mm × 100 mm × 6 mm with no groove joint geometry. The dilution was almost 0.8. The specimens were strictly cleaned by water rinsing, acid pickling, and polishing. Before welding, the welding specimens were cleaned by acetone and then abrased with steel brush to remove the grease and oxide on the surface of specimens. The plates were welded by tungsten inert gas arc welding (Fronius MW 4000, Austria) with two welding passes. The voltage and current of arc welding were 14 V and 280 A, respectively. The welding speed was 1.67 mm/s, and the arc gas was argon was 11 L/min flow rate. The parameters of the welding are listed in Table 2.

2.3 Characterization

X-ray diffraction analysis was performed to identify the phases in the fusion zone using Cu-Kα radiation at 40 kV and 40 mA with a speed of 6°/min (Model AXS-D8, Germany). The microstructures and morphologies of the fusion

Table 1 Nominal chemical composition (wt. %) of Al–Mg weld filler wires

Filler wire	Mg	Sc	Zr	Ti + B	Al
S5000	6.4–6.8	/	/	/	Bal
S5001	6.4–6.8	0.4	0.2	/	Bal
S5002	6.4–6.8	0.4	0.2	1.0–1.5	Bal

Table 2 Parameters of the welding

Filler wire	Welding current	Welding speed	Gas flow
S5000	280 A	1.67 mm/s	11 L/min
S5001	280 A	1.67 mm/s	11 L/min
S5002	280 A	1.67 mm/s	11 L/min

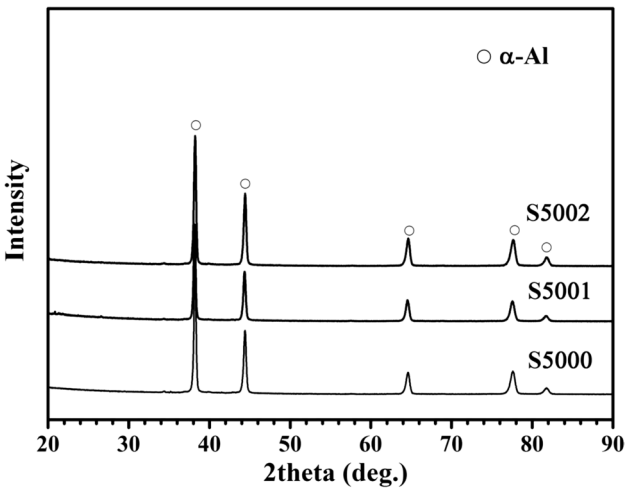

Fig. 1 X-ray diffraction pattern of the Al–Mg-Sc-Zr welded joint

zone and the heat-affected zone were characterized using optical microscopy (OM, Model DM4000M, Germany). The characterization of the second phase and Al matrix in the fusion zone was performed on an FEI Quanta 200F scanning electron microscope with energy-dispersive spectroscopy (EDS, Oxford Instruments Inc.). Transmission electron microscopy (TEM) samples of the Al–Mg-Sc-Zr welded joint were used to further identify the structure of the precipitated phase in the fusion zone and the heat-affected zone using a JEOL JEM-2100F microscope.

The tensile properties of welded joints with reinforcement and without reinforcement were tested at room temperature on a CMT-5105 electronic universal material testing machine with a tensile velocity of 2 mm/min. The impact tests were conducted by using a digital impact testing machine (HIT 50.PC, Germany) with the specimen dimensions of 55 mm × 10 mm × 6 mm. All tensile and impact test data were found by at least five parallel specimens to obtain the average value.

3 Results and discussions

3.1 Microstructure of the welded joint

Figure 1 shows the X-ray diffraction patterns of the S5000, S5001, and S5002 welded joints. These three welded joints exhibit similar X-ray diffraction profiles. The characteristic diffraction peaks of α-Al (PDF#04–0787) were detected in the Al–Mg-Sc-Zr welded joint, while the diffraction peaks of strengthening precipitates cannot be found because of the low content.

To investigate the effect of Zr/Sc and TiB_2 on the microstructure of Al–Mg-Sc-Zr welded joints, the optical micrograph and EBSD images of the fusion zone are presented in Figs. 2 and 3. The micrograph indicated that the Al–Mg-Sc-Zr welded joint can be divided into the fusion zone (FZ), the fusion line (FL), and the heat-affected zone (HAZ). Some dispersed precipitates with the angular morphology can be found in the fusion zone and heat-affected zone. These primary particles are suggested to be Al_3(Sc,Zr) as reported by Xu [23]. It can be seen that the microstructure of the S5000 weld with no refiner addition represents coarse equiaxed grains in the center of the welded joint and a columnar dendrite zone adjacent to the fusion line (FL), as presented in Figs. 2(a) and 3(a). With the addition of Zr and Sc increased to 0.6 wt. % in weld filler wires, the average grain size of S5001 welds decreased to 30 μm, as seen in Figs. 2(b) and 3(b). With the addition of TiB_2 in the fusion, the equiaxed grains with the lowest grain size of 10–20 μm were present in the fusion zone of the S5002 welded joint, as shown in Figs. 2(c) and 3(c).

The backscattered electron image in Fig. 4 was performed to observe the microstructures of the fusion zone in the Al–Mg-Sc-Zr welds. As seen in Fig. 4(a) and (b), the S5000 and S5001 welded joints had a uniform microstructure containing two clearly contrasting phases. The chemical composition of the phase was determined by EDS, confirming that the bright Al_3(Sc,Zr) particles with the size of 0.5 ~ 5 μm were uniformly dispersed on the gray α-Al matrix in the fusion zone. The fractions of the Al_3(Sc,Zr) particle were relative to the Sc and Zr content in the weld filler wire. For the S5002 welded joint presented in Fig. 4(c), a three-phase α-Al/Al_3Sc/TiB_2 microstructure can be observed in the fusion zone. The bright Al_3(Sc, Zr) and TiB_2 phases were evenly scattered on the gray α-Al matrix. Statistical analysis showed that most of the Al_3(Sc, Zr) and TiB_2 particles had the sizes of 1 ~ 10 μm.

Bright-field TEM micrographs in the center of the S5002 welded joint are shown in Fig. 5. In the center of the fusion zone, the phases with the size in the range of 100–120 nm can be found in the matrix grains, as seen in Fig. 5(a). The chemical analysis presented in Fig. 5(c) confirmed that Al, Sc, and Zr mainly exist in this triangular phase. The SAED patterns taken along the < 1 1 1 > direction exhibit that these precipitates are Al_3(Sc,Zr), as shown in Fig. 5(b). The irregular phases with the size of almost 500 nm can also be observed in the S5002 welded joint, as seen in Fig. 5(d). The lattice spots in the SAED pattern along the < 0 0 1 > direction and the chemical analysis,

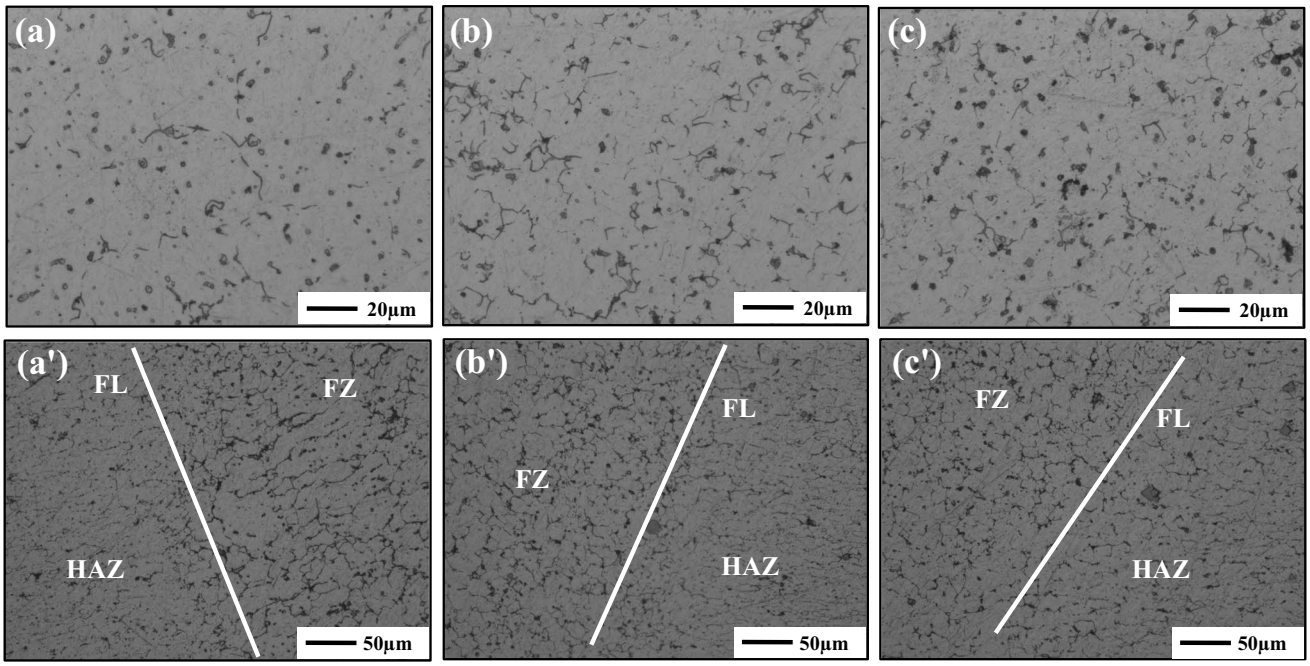

Fig. 2 Optical micrograph of fusion zone and heat-affected zone in weldment: S5000 (**a**) and (a′), S5001 (**b**) and (b′), and S5002 (**c**) and (c′)

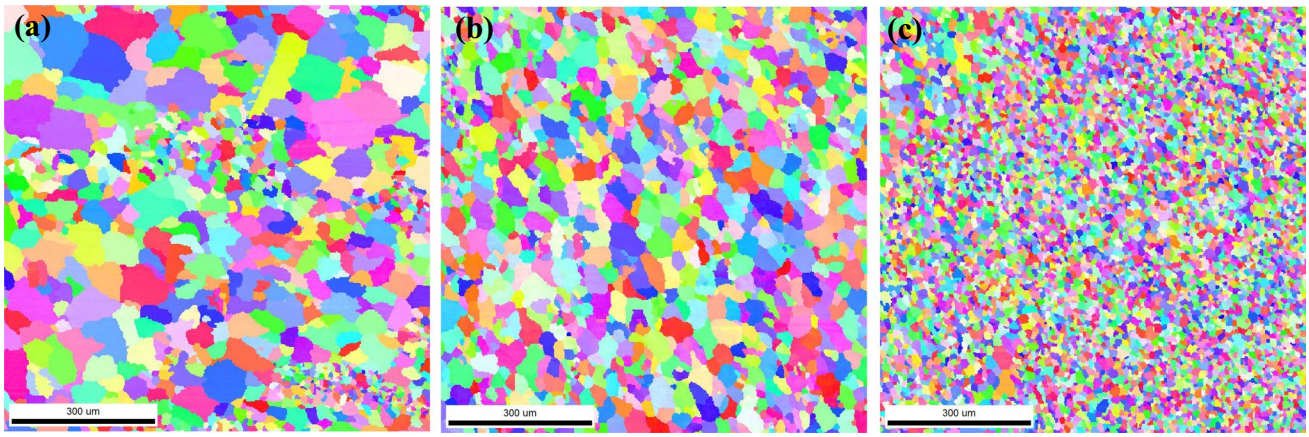

Fig. 3 EBSD images of fusion zone in S5000 (**a**), S5001 (**b**), and S5002 (**c**)

as seen in Fig. 5(e) and (f), demonstrated that the TiB_2 particles also exist in the fusion zone. Finally, the microstructure of the fusion zone in the S5002 weld was confirmed to be triangular $Al_3(Sc,Zr)$ and TiB_2 particles uniformly dispersed on the α-Al matrix. Figure 6 shows the TEM micrograph and corresponding SAED pattern of the sphere particles in the heat-affected zone of the Al–Mg-Sc-Zr welded joint. This sphere particle with the size of 10 ~ 50 nm is shown in Fig. 6(a). The SAED patterns taken along the $<0\ 1\ 1>_{Al}$ direction, as seen in Fig. 6(b), exhibit a number of $Al_3(Sc,Zr)$ with the size of 10 ~ 50 nm dispersed on the α-Al matrix in the heat-affected zone. The size of $Al_3(Sc,Zr)$ in the heat-affected zone slightly increased under the welding heat condition.

In this work, Sc and Zr are added into the base material and the weld filler wires. According to the phase diagram of the Al-Sc binary [23], the primary Al_3Sc particle cannot be formed during solidification unless the content Sc exceeds 0.55 wt. %, which is the eutectic composition. However, due to the existence of Zr, the eutectic composition is changed and the primary $Al_3(Sc,Zr)$ particles will be formed during solidification [28, 29].

As observed above, significant grain refinement due to the addition of Zr/Sc and TiB_2 has been shown to arise from

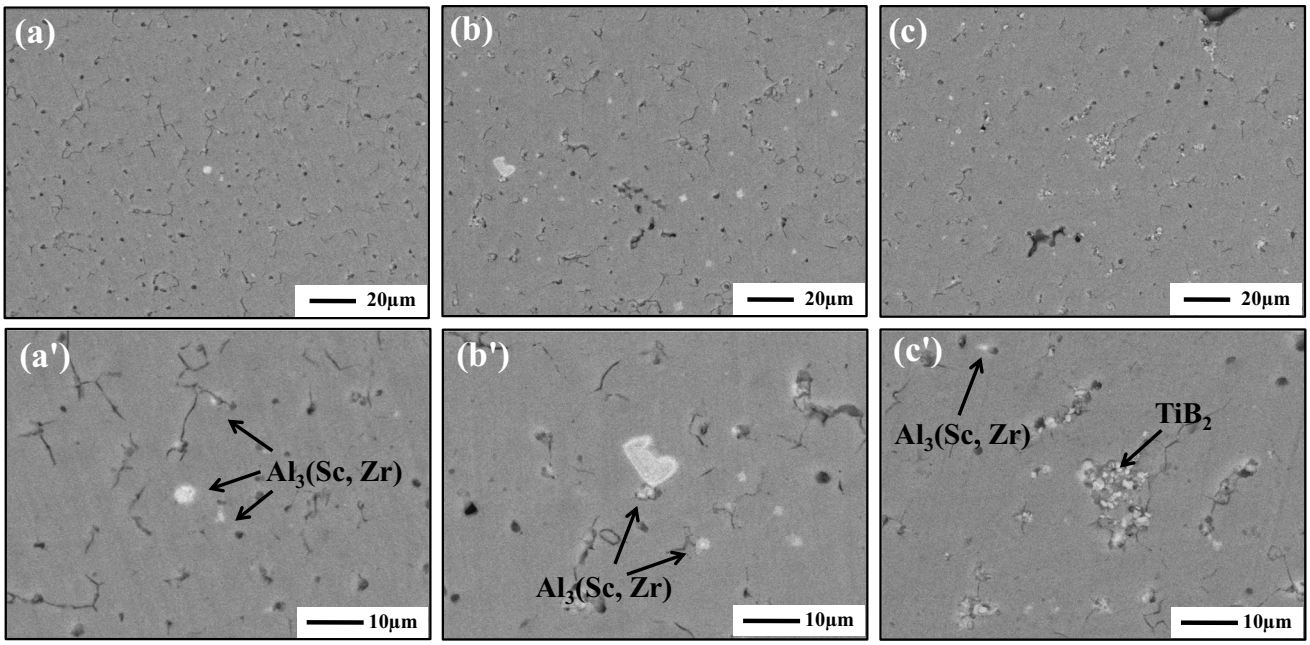

Fig. 4 Backscattered electron images of fusion zone in S5000 (**a**) and (a′), S5001 (**b**) and (b′), S5002 (**c**) and (c′)

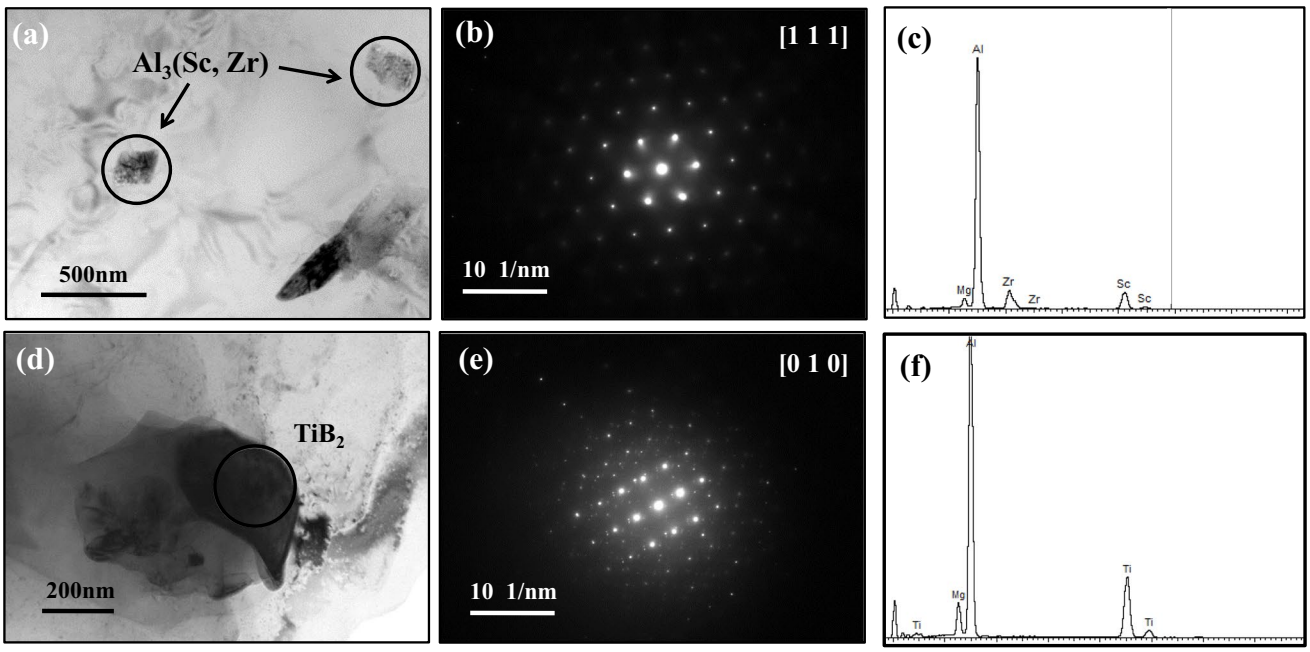

Fig. 5 TEM images of fusion zone in S5002 weld: (**a**) image of $Al_3(Sc,Zr)$ along < 1 1 1 >, (**b**) corresponding SAED pattern, (**c**) chemical analysis, (**d**) image of TiB_2 taken along < 0 1 0 > direction, (**e**) corresponding SAED pattern, and (**f**) chemical analysis

the primary $Al_3(Sc,Zr)$ and TiB_2 particles with the size of 0.1 ~ 5 μm which are presented within the α-Al grains. The similar crystal structure between the α-Al matrix and $Al_3(Sc,Zr)$ indicate that the aluminum has nucleated and grown epitaxially on these primary particles during the solidification, leading to the refinement of grain in the fusion zone [28]. For the refiner of the TiB_2 particle, previous studies [30] show that the nucleation of aluminum on the TiB_2 particles in the refiner appears at low undercooling, possibly by an adsorption mechanism. According to the nucleation model of $Al_3(Sc,Zr)$ and TiB_2, the inoculant particles located at the grains inside have the effects of hindering

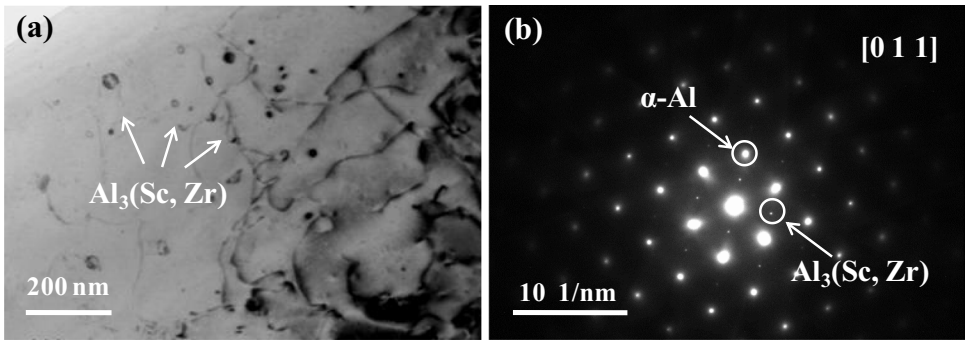

Fig. 6 TEM images of HAZ: (**a**) image of Al_3(Sc,Zr) along < 0 1 1 >, (**b**) corresponding SAED pattern

crystal growth and behaving as heterogeneous nucleation cites for aluminum grains, which refine the grain size in the fusion zone. In other words, there are no poisoning phenomena appearing in the combination of Al_3(Sc,Zr) and TiB_2 as the refiner.

3.2 Mechanical properties

The tensile tests were carried out for the base material and three welded joints with reinforcement and without reinforcement at room temperature. The yield strength and tensile strength of Al–Mg-Sc-Zr were 260 MPa and 410 MPa, repetitively. The yield strength, ultimate tensile strength, and elongation of the Al–Mg-Sc-Zr weld joints are shown in Table 3. It can be found that the yield strength and tensile strength of the Al–Mg-Sc-Zr welds with reinforcement were higher than those of the welded joints without reinforcement. The results of the tensile properties suggested that the yield strength and ultimate tensile strength of the Al–Mg-Sc-Zr welds increased with the addition of Zr/Sc and TiB_2. Consequently, the S5002 welded joint with 1 wt. % TiB_2 and 0.5 wt. % Zr/Sc displayed the best tensile properties. The yield strength and tensile strength of the S5002 welded joint with reinforcement reached 232.2 MPa and 386.3 MPa, and 208.0 MPa and 358.4 MPa for the S5002 welded joint without reinforcement, respectively. By comparing the elongation results of welded joints S5001 with S5000 and S5002, it can be concluded that the addition of TiB_2 did not have significant influence on plasticity.

In order to investigate the relationship between mechanical properties and fracture mechanism of the welded joint, the SEM fracture graphs of the tensile samples of the Al–Mg-Sc-Zr welded joints with reinforcement are presented in Fig. 7. The morphology of the fracture surface of S5000/S5001 and S5002 were observed to be different. The fracture occurred on the fusion zone adjacent to the fusion line (FL) for the S5000 and S5001 welded joints. It can be seen that the fine and uniform dimples of several microns distributed on the fracture surface, which exhibit a typical characteristic of the ductile fracture in the fusion zone of the S5001 weld, as seen in Fig. 7(b). For the S5002 weld with addition of the TiB_2 particle, the fracture occurred on the heat-affected zone, revealing a good mechanical property of the welded joint. It was noted that the mode of fracture surface morphology is ductile and consists of voids and well-developed dimples, as shown in Fig. 7(c). In contrast, all the three welds without reinforcement ruptured in the fusion zone during the stretching process, representing a similar fracture graph, as seen in Fig. 8. The fine and uniform microvoids were observed on the fracture surface of the Al–Mg-Sc-Zr welded joint, which shows a tendency of ductile fracture, as seen in Fig. 8(a)-(c). It can be concluded that the fracture behavior of the welded joints changed with the content of weld filler wires, and the S5002 welded joint with 1 wt. % TiB_2 and 0.5 wt. % Zr/Sc has a better tensile property.

Table 4 shows the impact toughness (α_k) of the Al–Mg-Sc-Zr weldments. It was shown that the S5001 weldment exhibits the best properties of impact toughness, i.e., its

Table 3 Tensile properties of the Al–Mg-Sc welded joint

Filler wire #	Statement	Yield strength (MPa)	Ultimate tensile strength (MPa)	Elongation (Pct)
S5000	With reinforcement	224.5	365.4	10.1
S5001	With reinforcement	230.6	383.2	14.5
S5002	With reinforcement	232.2	386.3	15.1
S5000	Without reinforcement	193.0	329.9	8.7
S5001	Without reinforcement	200.7	350.5	12.7
S5002	Without reinforcement	208.0	358.4	12.2

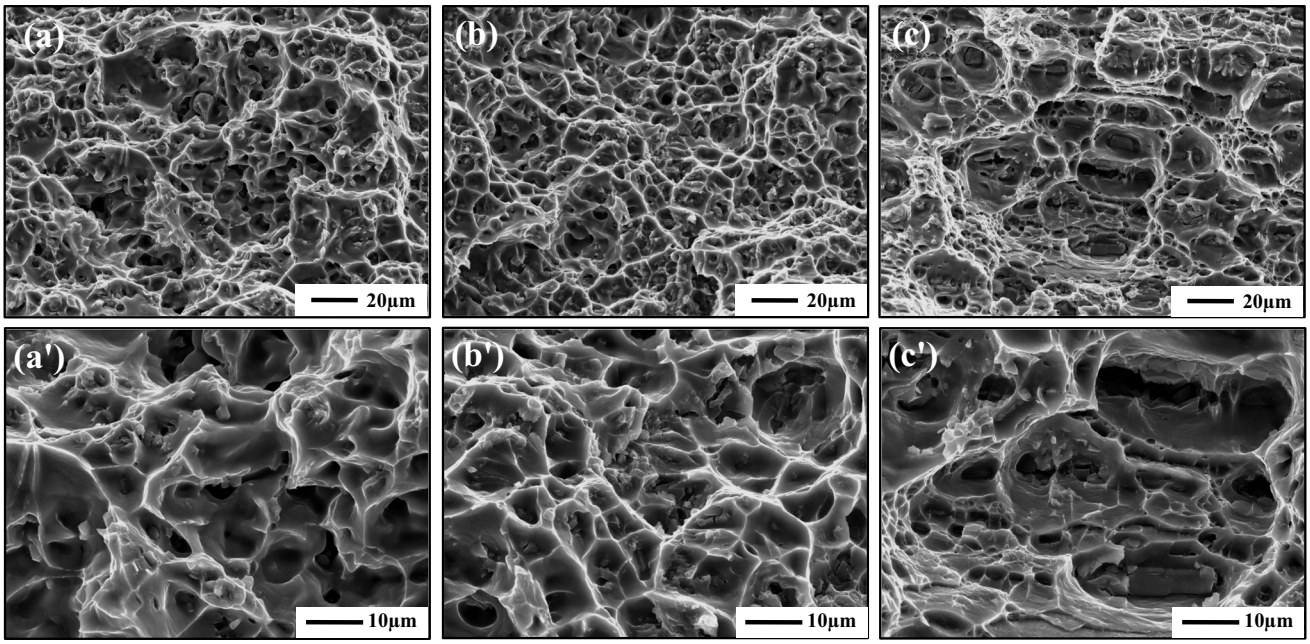

Fig. 7 SEM micrographs of the tensile fracture surfaces of Al–Mg-Sc-Zr welded joints with reinforcement: S5000 (**a**) and (a′), S5001 (**b**) and (b′), S5002 (**c**) and (c′)

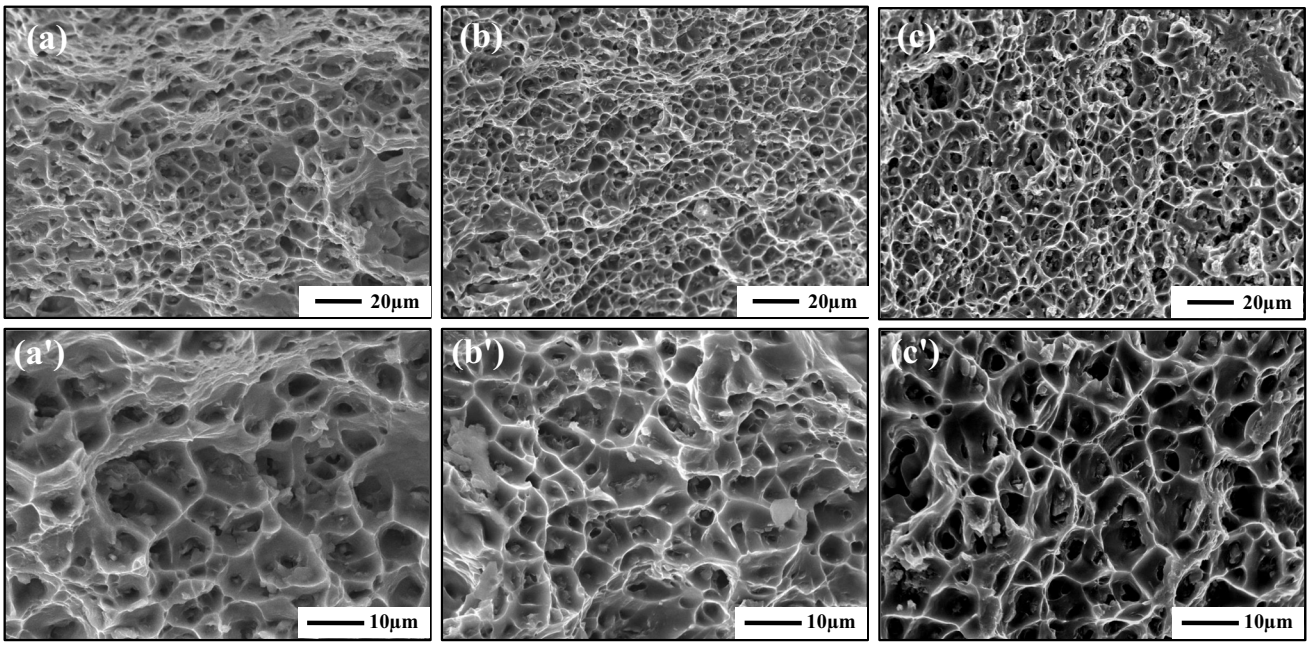

Fig. 8 SEM micrographs of the tensile fracture surfaces of Al–Mg-Sc-Zr welded joints without reinforcement: S5000 (**a**) and (a′); S5001 (**b**) and (b′); S5002 (**c**) and (c′)

impact toughness was higher than 37 J/cm^2. This result suggests that Zr/Sc addition in the weld filler wire can slightly improve the impact toughness of the Al–Mg-Sc-Zr welded joint. The effect of TiB_2 content on impact toughness was contrary to the tensile strength. With the same content of Zr and Sc in the filler wire, the impact toughness slightly decreased with the addition of the TiB_2 particle into the fusion melt.

The welded joints without reinforcement ruptured in the fusion zone nearby the fusion boundary, suggesting

Table 4 Impact properties of the Al–Mg-Sc welded joint

Filler wire #	Fracture toughness (α_k, J/cm^2)
S5000	36.7
S5001	38.1
S5002	34.0

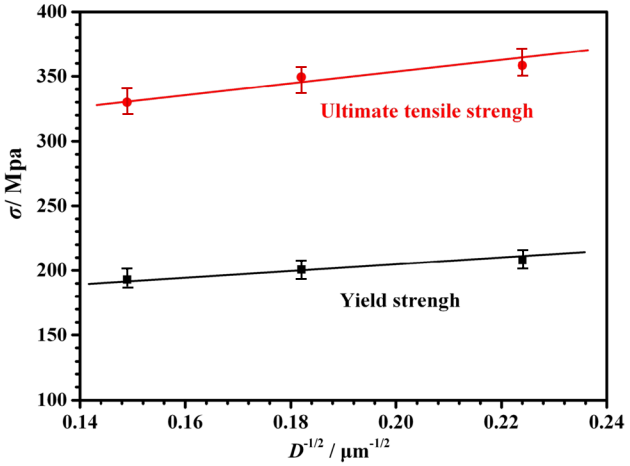

Fig. 9 Tensile strength (σ) of the Al–Mg-Sc-Zr welded joint plotted against grain size ($D^{-1/2}$)

that the fusion zone is weaker than the heat-affected zone and base material. It has been researched in previous works that a high density of $Al_3(Sc,Zr)$ with the size of 5 ~ 10 nm is dispersed in the base metal, providing a greater strengthening effect [23]. It can be said that a low density of coarse refiner in the fusion zone leads to the decrease in tensile properties, i.e., the coefficients of yield strength and ultimate tensile strength of welded joints without reinforcement are almost 0.80 and 0.85. The results of the tensile test also proved that the addition of Zr/Sc and TiB_2 increases the yield strength and the ultimate tensile strength, meaning that the microstructure in the fusion zone is very important to the tensile properties of Al–Mg-Sc-Zr weldment.

The relationship between the tensile strength (yield strength and the ultimate tensile strength) and the grain size ($D^{-1/2}$) of the Al–Mg-Sc-Zr welded joint is consistent with the Hall–Petch equation [31]:

$$\sigma_b = \sigma_0 + k_b D^{-1/2} \quad (1)$$

where σ_b is tensile strength, σ_0 is the Peierls-Nabarro stress, D is the grain size of the welded joint, and k_b is the slope. The tensile strength of the welded joint plotted against grain size ($D^{-1/2}$) is shown in Fig. 9. The k_b values of the yield strength and the ultimate tensile strength are 200 MPa·μm$^{-1/2}$ and 402 MPa·μm$^{-1/2}$, respectively. This linear relationship between tensile strength and grain size ($D^{-1/2}$) suggests that addition of refiner such as Zr/Sc and TiB_2 can improve the tensile strength.

To further investigate the effect of grain refiner on the mechanical properties of the Al–Mg-Sc-Zr welded joint, the welding specimens were machined to the dimension of 150 mm × 100 mm × 6 mm with a V-groove joint geometry to increase the content of the grain refiner such as $Al_3(Sc,Zr)$ and TiB_2. The Al–Mg-Sc-Zr specimen was welded using S5002 weld filler wires. The welded joint displayed the best tensile property; its yield strength and tensile strength of the welded joint without reinforcement reached 222.0 MPa and 362.3 MPa, as seen in Table 5. This result further proved that the tensile strength and yield strength of the Al–Mg-Sc-Zr welded joint increase with the increase of grain refiner content in the fusion.

4 Conclusions

The Al–Mg-Sc-Zr alloy was welded using the weld filler wires containing different additions of Zr, Sc, and TiB_2. The effect of addition of Zr, Sc, and TiB_2 on the microstructure and mechanical behaviour of the welded joint with reinforcement and without reinforcement was investigated.

1) The microstructure of the fusion zone in the Al–Mg-Sc-Zr welded joint consists of α-Al matrix, $Al_3(Sc,Zr)$, and TiB_2 particles (S5002). The fractions of the $Al_3(Sc,Zr)$ particle were relative to the Sc and Zr content in weld filler wire.
2) The $Al_3(Sc,Zr)$ and TiB_2 particles located at the grains inside have the effects of hindering crystal growth and behaving as heterogeneous nucleation sites for aluminum grains, which refine the grain size in the fusion zone.
3) The relationship between the tensile strength and the grain size of the welded joint is consistent with the linear

Table 5 Tensile properties of the Al–Mg-Sc-Zr welded joint (V-groove joint geometry)

Filler wire #	Statement (V-groove)	Yield strength (MPa)	Ultimate tensile strength (MPa)	Elongation (Pct)
S5002	With reinforcement	235.8	388.6	15.3
S5002	Without reinforcement	223.6	363.4	11.8

equation. The tensile strength and yield strength of the Al–Mg-Sc-Zr welded joint increase with the decrease in grain size in the fusion zone.

4) With a uniform $Al_3(Sc,Zr)$ and TiB_2 dispersed on the α-Al matrix, the S5002 weld displayed the best tensile property. Its yield strength and ultimate tensile strength reached 232.2 MPa and 386.3 MPa with reinforcement, and the yield strength and tensile strength of welded joint without reinforcement were about 208.0 MPa and 358.4 MPa, respectively.

Declarations

Conflict of interest The authors declare no competing interests.

References

1. Wen SP, Xing ZB, Huang H, Li BL, Wang W, Nie ZR (2009) The effect of erbium on the microstructure and mechanical properties of Al-Mg-Mn-Zr alloy. Mater Sci Eng A 516:42–49
2. Zha M, Li Y, Mathiesen RH, Bjørge R, Roven HJ (2014) Achieve high ductility and strength in an Al-Mg alloy by severe plastic deformation combined with inter-pass annealing. Mater Sci Eng A 598:141–146
3. Alil A, Popović M, Radetić T, Zrilić M, Romhanji E (2015) Influence of annealing temperature on the baking response and corrosion properties of an Al-4.6 wt% Mg alloy with 0.54 wt% Cu. J Alloys Compd 625:76–84
4. Li MJ, Pan QL, Shi YJ, Wang Y (2014) Microstructure dependent fatigue crack growth in Al-Mg-Sc alloy. Mater Sci Eng A 611:142–151
5. Lathabai S, Lloyd PG (2002) The effect of scandium on the microstructure, mechanical properties and weldability of a cast Al-Mg alloy. Acta Mater 50:4275–4292
6. Mousavi MG, Cross CE, Grong Ø (1999) Effect of scandium and titanium–boron on grain refinement and hot cracking of aluminium alloy 7108. Sci Technol Weld Join 4:381–388
7. Schempp P, Rethmeier M (2015) Understanding grain refinement in aluminium welding. Weld World 59:767–784
8. Coniglio N, Cross CE (2009) Mechanisms for solidification crack initiation and growth in aluminum welding. Metall Mater Trans A 40:2718–2728
9. Cross CE, Grong O, Mousavi M (1999) A model for equiaxed grain formation along the weld metal fusion line. Scrip. Mater. 40.
10. Dvornak MJ, Frost RH, Olson DL (1991) Influence of solidification kinetics on aluminum weld grain refinement. Weld J 70:271–276
11. Schempp P, Cross CE, Häcker R et al (2013) Influence of grain size on mechanical properties of aluminium GTA weld metal. Weld World 57:293–304
12. Schempp P, Cross CE, Schwenk C et al (2012) Influence of Ti and B additions on grain size and weldability of aluminium alloy 6082. Weld World 56:95–104
13. Schempp P, Schwenk C, Rethmeier M et al (2011) Weld metal grain refinement of aluminium alloy 5083 through controlled additions of Ti and B. Mater Test 53:604–609
14. Schempp P, Cross CE, Pittner A et al (2013) Influence of solute content and solidification parameters on grain refinement of aluminum weld metal. Metall Mater Trans A 44:3198–3210
15. Schempp P, Cross CE, Pittner A et al (2014) Grain structure in aluminium TIG welds. Weld Cut 13:177–181
16. Røyset J, Ryum N (2005) Scandium in aluminium alloys. Int Mater Rev 50:19–44
17. Drits M, Toporova L, Bykov Y, Yelagin V, Filatov Z (1982) Structure and properties of Al-Sc and Al-Mg-Sc alloys, Met. and Metalloved. Cvet. Metall. 213–223.
18. Costa S, Puga H, Barbosa J, Pinto AMP (2012) The effect of Sc additions on the microstructure and age hardening behaviour of as cast Al-Sc alloys. Mater Des 42:347–352
19. Filatov YA, Yelagin VI, Zakharov VV (2000) New Al-Mg-Sc alloys. Mater Sci Eng A 280:97–101
20. Marquis EA, Seidman DN, Asta M, Woodward C (2006) Composition evolution of nanoscale Al_3Sc precipitates in an Al-Mg-Sc alloy: experiments and computations. Acta Mater 54:119–130
21. Lee S, Utsunomiya A, Akamatsu H, Neishi K, Furukawa M, Horita Z, Langdon T (2002) Influence of scandium and zirconium on grain stability and superplastic ductilities in ultrafine-grained Al-Mg alloys. Acta Mater 50:553–564
22. Jiang F, Zhou J, Huang H, Qu J (2015) Characterisation of microstructure and mechanical properties in Al-Mg alloy with addition of Sc and Zr. Mater Res Innov 18:228–234
23. Xu P, Jiang F, Meng S et al (2018) Microstructure and mechanical properties of Al-Mg-Sc-Zr alloy variable polarity plasma arc welding joint. J Mater Eng Perform 27:4783–4790
24. Muñoz AC, Rückert G, Huneau B, Sauvage X, Marya S (2008) Comparison of TIG welded and friction stir welded Al-4.5Mg-0.26Sc alloy. J Mater Process Techno 197:337–343
25. Malinkina TI, Markachev NA, KovtunA VA et al (1998) Welded structures of 01570 aluminium alloy[J]. Weld Inter 12(7):566–569
26. Fu L, Peng YY, Huang JW, Deng Y, Yin ZM (2015) Microstructures and mechanical properties of gas tungsten arc welded joints of new Al-Mg-Sc and Al-Mg-Er alloy plates. Mater Sci Eng A 620:149–154
27. Jiang F, Chen SL, Huang BY, Yin ZM, He YH (2005) Microstructure and properties of Al-Mg-(Sc, Zr) welded joint. J Cent South Univ Techno 12:23–27
28. Zhou SA, Zhang Z, Li M (2016) Effect of Sc on microstructure and mechanical properties of as-cast Al-Mg alloys. Mater Des 90:1077–1084
29. Yin Z, Pan Q, Zhang Y et al (2000) Effect of minor Sc and Zr on the microstructure and mechanical properties of Al–Mg based alloys. Mater Sci Eng A 280:151–155
30. Greer AL, Bunn AM et al (2000) Modelling of inoculation of metallic melts: application to grain refinement of aluminium by Al-Ti-B. Acta Mater 48:2823–2835
31. Li XW, Cai QZ, Zhao BY, Xiao YT, Li B (2016) Effect of nano TiN/Ti refiner addition content on the microstructure and properties of as-cast Al-Zn-Mg-Cu alloy. J Alloy Compd 675:201–210